Flow properties and hydrodynamic interactions of rigid spherical microswimmers

Tapan Chandra Adhyapak* and Sara Jabbari-Farouji†
Institut für Physik, Johannes Gutenberg-Universität Mainz, Staudingerweg 7-9, 55128 Mainz, Germany
(Received 8 June 2017; published 27 November 2017)

We analyze a minimal model for a rigid spherical microswimmer and explore the consequences of its extended surface on the interplay between its self-propulsion and flow properties. The model is the first order representation of microswimmers, such as bacteria and algae, with rigid bodies and flexible propelling appendages. The flow field of such a microswimmer at finite distances significantly differs from that of a point-force (Stokeslet) dipole. For a suspension of microswimmers, we derive the grand mobility matrix that connects the motion of an individual swimmer to the active and passive forces and torques acting on all the swimmers. Our investigation of the mobility tensors reveals that hydrodynamic interactions among rigid-bodied microswimmers differ considerably from those among the corresponding point-force dipoles. Our results are relevant for the study of collective behavior of hydrodynamically interacting microswimmers by means of Stokesian dynamics simulations at moderate concentrations.

DOI: 10.1103/PhysRevE.96.052608

I. INTRODUCTION

Microswimmers have attracted a lot of attention from soft matter physicists recently [1–6]. Intensive research has been directed towards living microswimmers such as bacteria [7–16], algae [17,18], and other microorganisms [19–22]. Moreover, physicists' contributions have reached beyond just living systems, and studies on artificial microswimmers have also been increasing [23–25]. Microswimmers are the prime examples of active particles [26]. Their individual dynamics involves challenging physics [27–31], and their collective behaviors often exhibit surprises that have triggered a number of new directions in physics per se [2–4,32].

Microswimmers immersed in a viscous fluid generate long-range flows as they move. They also experience hydrodynamic interactions as they react to the local flow generated by the others. Many distinctive dynamical features of microswimmers result from the interplay between their self-propulsion and mutual hydrodynamic interactions [2,17,33,34]. However, the consequences of hydrodynamic interactions on their dynamics are not fully understood. Although the importance of the particle size and shape on the hydrodynamics of passive objects is well known [35,36], the influence of the finite body size on the swimming behavior of active particles has received little attention [37–39].

Most studies of collective behavior treat microswimmers as hydrodynamic point-force (Stokeslet) dipoles [1,37,40]. This approximation accounts for the hydrodynamic interactions correctly at very dilute concentrations where the body size of the individual swimmers is negligible with respect to the interparticle separations. Here we analyze a minimal model for a rigid spherical microswimmer by incorporating the influence of its extended surface on the flow created during the self-propulsion. We thereby investigate the role of the finite-body size on its locomotion, flow properties, and the hydrodynamic interactions with other swimmers.

Our microswimmer model consists of a spherical cell body of radius a self-propelled with a constant force $\mathbf{f}^{\mathrm{sp}}$. The force neutrality implies that a force with the same magnitude f^{sp} and with the opposite direction acts on the fluid at a distance ℓ from its center of mass; see Fig. 1 for a schematics of the model. Although a similar model has been proposed before in Ref. [38], its flow field and the hydrodynamic interactions have been calculated only in the limit of $a/\ell \to 0$. Here we obtain the flow field of such a swimmer for arbitrary values of a/ℓ by employing the method of image systems [36].

Our study shows that the flow field of a rigid-bodied spherical microswimmer with a finite a/ℓ differs from that of a point-force dipole both qualitatively and quantitatively. The magnitude and the angular dependence of the flow field deviate from that of a point-force dipole even at distances significantly larger than the swimmer's size. Remarkably, the front-back symmetry of the flow field with respect to the self-propulsion direction is broken. Eventually, at very large distances the flow field of this model converges to that of a point-force dipole. Nevertheless, its dipole strength S^{eff} is different from $f^{\mathrm{sp}}\ell$, i.e., the dipole strength in the limit $a/\ell \to 0$. Instead, it is given by $S^{\mathrm{eff}} = f^{\mathrm{sp}}\ell^{\mathrm{eff}}$ in which $\ell^{\mathrm{eff}} < \ell$.

The calculation of the flow field allows us to investigate the influence of the finite body size on the hydrodynamic interactions. For this purpose, we derive the *grand* mobility tensor that connects the linear and angular velocities of the swimmers to the active and passive forces and torques acting on them. We find that the leading order far-field hydrodynamic interactions among the microswimmers are the same as those among point-force dipoles when we renormalize the dipole strengths of the latter to S^{eff}. However, the next leading order terms do not agree even at far distances unless $a/\ell \to 0$. The explicit expressions for the mobility tensor allow us to employ Stokesian dynamics simulations [41] for exploring the collective behavior of rigid-bodied microswimmers at experimentally relevant concentrations.

Before we proceed, we point out that there are other studies besides Ref. [38] mentioned above that have investigated the flow fields and hydrodynamic interactions of microswimmers with finite bodies [37,39,42–48]. Menzel *et al.* [39] have

*tadhyapa@uni-mainz.de
†sjabbari@uni-mainz.de

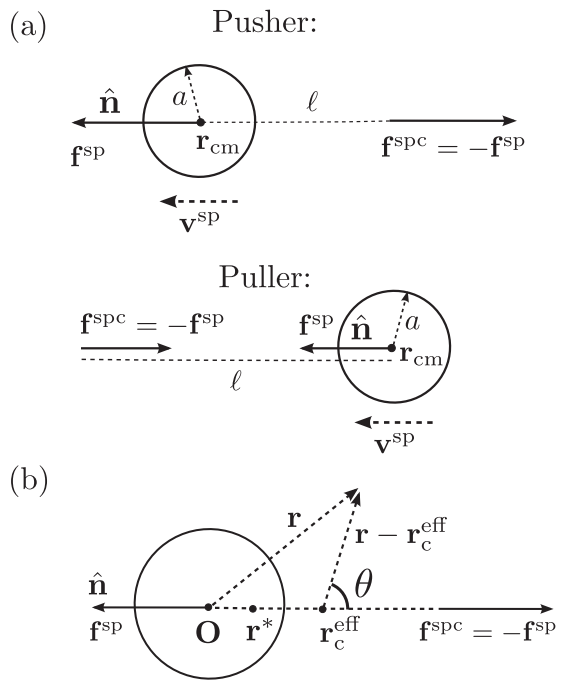

FIG. 1. (a) Schematics of our minimal model for a spherical swimmer of radius a. The swimmer is driven by an active force $\mathbf{f}^{\rm sp} = f^{\rm sp}\hat{\mathbf{n}}$ directed along its intrinsic orientation $\hat{\mathbf{n}}$. Force neutrality of the system is incorporated via a conjugate force $\mathbf{f}^{\rm spc} = -\mathbf{f}^{\rm sp}$ that acts on the fluid at the position $\mathbf{r}_{\rm c} = \mathbf{r}_{\rm cm} \pm \ell\hat{\mathbf{n}}$ where $\mathbf{r}_{\rm cm}$ is the center of mass of the spherical body. For a pusher (top), $\mathbf{r}_{\rm c} = \mathbf{r}_{\rm cm} - \ell\hat{\mathbf{n}}$ and the forces $\mathbf{f}^{\rm sp}$ and $\mathbf{f}^{\rm spc}$ point away from each other, whereas for a puller (bottom), $\mathbf{r}_{\rm c} = \mathbf{r}_{\rm cm} + \ell\hat{\mathbf{n}}$, the forces point towards each other. (b) The model swimmer in a coordinate system whose origin $\mathbf{O}$ coincides with the swimmer's center of mass $\mathbf{r}_{\rm cm}$. $\mathbf{r}$ denotes any point in the fluid and $\mathbf{r}_{\rm c}^{\rm eff}$ the center of the effective point-force dipole that produces the same flow in the far field as the swimmer. Any point in the x-y plane containing the vector $\hat{\mathbf{n}} = -\hat{\mathbf{x}}$ can also be denoted by the vector $\mathbf{r} - \mathbf{r}_{\rm c}^{\rm eff}$, which originates from $\mathbf{r}_{\rm c}^{\rm eff}$ and makes an angle θ with $\hat{\mathbf{x}}$. The point $\mathbf{r}^* = -(a^2/\ell)\hat{\mathbf{n}}$ denotes the position of the hydrodynamic image systems of the point force $\mathbf{f}^{\rm spc}$ generated by the sphere.

proposed a spherical swimmer model with two equal and opposite point forces that act directly on the fluid where the swimmer's body is placed asymmetrically between the two forces. The authors also have disentangled the contributions of active and passive forces to the mobility tensor. However, they have neglected the hydrodynamic contributions of the image systems of the point forces near the swimmer's body in their calculations. Furthermore, similar swimmer models with finite size and elongated body driven by two point forces have been studied numerically using the Lattice-Boltzmann simulation method by Graaf *et al.* [47].

The remainder of paper is organized as follows. In Sec. II we introduce the minimal swimmer model and examine its dynamics and flow field in detail. The Sec. III is devoted to the hydrodynamic interactions between different swimmers. Finally, we conclude our work in Sec. IV where we summarize our main findings and discuss the consequences of the finite body size on the dynamics of the swimmers.

II. MINIMAL MODEL FOR A SPHERICAL SWIMMER AND ITS DYNAMICS

We first introduce our model for the simplest realization of rigid-bodied spherical microswimmers. Then we analyze the flow properties of an individual swimmer in both the absence and the presence of external forces and torques.

A. Model description

Our minimal microswimmer model consists of a rigid spherical body with hydrodynamic radius a suspended in a fluid of viscosity η. The swimmer has an intrinsic orientation $\hat{\mathbf{n}}$ defined by its self-propulsion direction. We assume that no active torque acts on the swimmer and the self-propulsion is provided by an internal force $\mathbf{f}^{\rm sp} = f^{\rm sp}\hat{\mathbf{n}}$. As a working rule of the rigid body dynamics, $\mathbf{f}^{\rm sp}$ can be considered to be acting on any arbitrary point along $\hat{\mathbf{n}}$, especially on the center of mass $\mathbf{r}_{\rm cm}$. However, in Sec. II B 3 we show that the effective point of action of $\mathbf{f}^{\rm sp}$ is actually slightly shifted from $\mathbf{r}_{\rm cm}$.

There are a multitude of mechanisms for the generation of self-propulsion adopted by various microswimmers. In all the cases there is an internal cycle of period τ that repeats itself to generate the propulsion. The force $\mathbf{f}^{\rm sp}$ then represents the thrust experienced by a microswimmer when averaged over time $t \gg \tau$. On such time scales the force-free condition for a swimmer is satisfied by introducing a point force $\mathbf{f}^{\rm spc} = -\mathbf{f}^{\rm sp}$ acting on the fluid at the position $\mathbf{r}_{\rm cm} \pm \ell\hat{\mathbf{n}}$ where $\ell > a$. The plus sign describes a puller-type swimmer and the minus sign corresponds to a pusher type. A schematics of our model swimmer is presented in Fig. 1(a).

Relating to a real microswimmer, in the case of a flagellated bacterium, for example, $\mathbf{f}^{\rm spc}$ can be interpreted as the time averaged force exerted by its flagella on the fluid, and $\mathbf{f}^{\rm sp}$ is the resulting thrust force on the body of the bacterium. For real microorganisms, $\mathbf{f}^{\rm spc}$ is distributed over an extended region in the fluid. Our model treats these forces minimally as an effective hydrodynamic force acting at a single point on the fluid that lies at a distance ℓ from $\mathbf{r}_{\rm cm}$ and neglects the details of the force distribution to a first order approximation. The distance ℓ remains as a free parameter in the model that can be interpreted as the distance from the center of mass of the body to an effective action point of the hydrodynamic forces on the fluid.

Due to their small sizes and low speeds, microswimmers move in the realm of low Reynolds numbers. Hence, we can neglect inertial effects on both the dynamics of the fluid and that of the microswimmers [49]. In this limit, the flow field is described by the incompressible Stokes equation, and the microswimmer's dynamics is controlled by force and torque balance equations given by

$$\mathbf{F}^h + \mathbf{f}^{\rm sp} + \mathbf{f}^{\rm ext} = 0, \tag{1}$$

$$\mathbf{L}^h + \mathbf{L}^{\rm ext} = 0, \tag{2}$$

where $\mathbf{F}^h$ and $\mathbf{L}^h$ are the total force and torque exerted by the surrounding fluid on the swimmer. $\mathbf{f}^{\rm ext}$ and $\mathbf{L}^{\rm ext}$ are, respectively, the net external force and torque experienced by it. In the following, we analyze the motion of a swimmer in the absence and presence of external forces and torques.

B. Dynamics of a free swimmer

We first focus on the dynamics of a free microswimmer, i.e., one on which no external forces or torques are exerted. We obtain the self-propulsion velocity in terms of the model parameters. Then we discuss the microswimmer's flow field and its far-field behavior.

1. Self-propulsion velocity

In order to obtain the net self-propulsion velocity of the free swimmer $\mathbf{v}^{\rm sp}$, we assume that the fluid velocity on the surface of the spherical body satisfies the stick boundary conditions. Hence, the velocity of any point $\mathbf{r}_S$ on its surface S is equal to the local fluid velocity at that point:

$$\mathbf{v}^{\rm sp} = -\oint_S dS'\, \mathbf{T}(\mathbf{r}_S - \mathbf{r}'_S)\cdot\mathbf{f}(\mathbf{r}'_S) + \mathbf{u}_0(\mathbf{r}_S), \tag{3}$$

where $\mathbf{T}(\mathbf{r}) = (1/8\pi\eta r)(\mathbf{I} + \mathbf{rr}/r^2)$ is the Oseen tensor, and $\mathbf{u}_0(\mathbf{r}) = -\mathbf{T}(\mathbf{r} - \mathbf{r}_{\rm cm} \pm \ell\hat{\mathbf{n}})\cdot\mathbf{f}^{\rm sp}$ is the flow field because of the point force $\mathbf{f}^{\rm spc}$ acting on the fluid. Here $+$ and $-$ denote a pusher and puller type of swimmer, respectively. $\mathbf{f}(\mathbf{r}_S)$ is the force per unit area exerted by the fluid on the swimmer's surface at $\mathbf{r}_S$. Note that $\mathbf{f}(\mathbf{r}_S)$ acquires a contribution from the fluid flow created by the point force $\mathbf{f}^{\rm spc}$. Thus, it is not uniform over the spherical surface as it would have been in the absence of $\mathbf{f}^{\rm spc}$ [35]. Furthermore, the angular velocity of the swimmer does not appear in Eq. (3) because no external torque acts on the body and the flow $\mathbf{u}_0$ does not generate any rotation of the swimmer [50].

Integrating both sides of Eq. (3) over the surface of the swimmer and utilizing the spherical symmetry of the body [51], we obtain

$$\mathbf{v}^{\rm sp} = -\frac{1}{6\pi\eta a}\oint_S dS'\,\mathbf{f}(\mathbf{r}'_S) + \frac{1}{4\pi a^2}\oint_S dS\,\mathbf{u}_0(\mathbf{r}_S), \tag{4}$$

where $\oint_S dS'\,\mathbf{f}(\mathbf{r}'_S)$ is equal to the net hydrodynamic force $\mathbf{F}^{\rm h}$ on the sphere. The force balance condition, Eq. (1), for a free swimmer thus implies that $\oint_S dS'\,\mathbf{f}(\mathbf{r}'_S) = -\mathbf{f}^{\rm sp}$. The second integral above can be calculated by a Taylor expansion of the flow field around $\mathbf{r}_{\rm cm}$ [35]. Because of the spherical symmetry of the swimmer the Taylor expansion truncates at the quadratic order in a. Thus, Eq. (4) simplifies to the exact expression,

$$\mathbf{v}^{\rm sp} = \frac{1}{6\pi\eta a}\mathbf{f}^{\rm sp} + \left(1 + \frac{a^2}{6}\nabla^2_{r_{\rm cm}}\right)\mathbf{u}_0(\mathbf{r}_{\rm cm}). \tag{5}$$

This equation is identical to the familiar Faxen's law [35]. Evaluating $\nabla^2_{r_{\rm cm}}\mathbf{u}_0(\mathbf{r}_{\rm cm})$ explicitly, we obtain the self-propulsion velocity in terms of a and ℓ:

$$\mathbf{v}^{\rm sp} = \frac{1}{6\pi\eta a}\{1 - g_{a/\ell}\}\mathbf{f}^{\rm sp}, \tag{6}$$

in which $g_{a/\ell} \equiv (3/2)[a/\ell - (a/\ell)^3/3]$. Since $0 < g \leqslant 1$ for the physically relevant range $0 < a/\ell \leqslant 1$, the swimmer's velocity is in the direction of $\mathbf{f}^{\rm sp}$, as expected. Furthermore, owing to the symmetry of the Oseen tensor $\mathbf{T}(+\ell\hat{\mathbf{n}}) = \mathbf{T}(-\ell\hat{\mathbf{n}})$, for a given set of parameters (a,ℓ), the self-propulsion speeds of a pusher and a puller are identical.

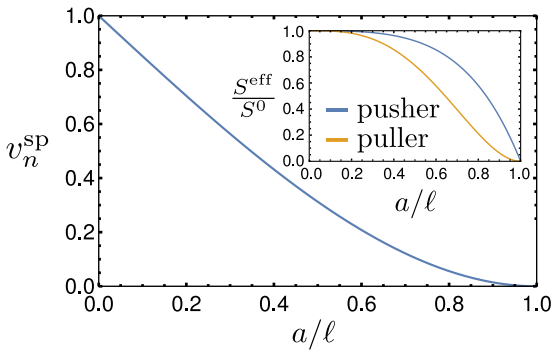

FIG. 2. The normalized swimming speed $v_n^{\rm sp} = v^{\rm sp}/(f^{\rm sp}/6\pi\eta a)$ of a spherical swimmer of radius a, plotted against a/ℓ, where ℓ is the separation between the active forces $\mathbf{f}^{\rm sp}$ and $\mathbf{f}^{\rm spc} = -\mathbf{f}^{\rm sp}$. The plots of $v_n^{\rm sp}$ for both pushers and pullers are identical. Inset: The ratio $S^{\rm eff}/S^0$ of the dipole strengths of the *effective* point-force dipole producing the correct far field and the point-force dipole obtained in the limit of zero swimmer size.

In Fig. 2 we have presented the normalized swimming speed $v_n^{\rm sp} = v^{\rm sp}/(f^{\rm sp}/6\pi\eta a)$ versus a/ℓ. We note that $v_n^{\rm sp}$ is a decreasing function of a/ℓ. In the limit of $a \ll \ell$, the speed of the swimmer approaches to that of a sphere dragged by a single isolated force $f^{\rm sp}$, i.e., $v^{\rm sp} \to f^{\rm sp}/6\pi\eta a$. However, for $a/\ell \geqslant 0.4$, a range relevant for some of flagellated bacteria, the value of $v_n^{\rm sp}$ is considerably smaller than one. Thus the flow created by the neutralizing force $\mathbf{f}^{\rm spc}$ results in a considerable lowering of the speed of the swimmer compared to its passive counterpart, an externally driven sphere.

2. Flow field

Next, we obtain the flow field of a spherical swimmer and compare it to that of a point-force dipole. To calculate the flow field $\mathbf{u}(\mathbf{r})$ of the swimmer, we need to incorporate two contributions: (a) the flow field $\mathbf{u}_a$ generated because of the point force $\mathbf{f}^{\rm spc}$ that lies near a sphere and (b) the flow $\mathbf{u}_b$ resulting from the translation of the sphere with velocity $\mathbf{v}^{\rm sp}$ in an otherwise quiescent flow. In the following, we obtain each of these contributions for a sphere centered at the origin $\mathbf{O}$.

$\mathbf{u}_a$ can be expressed as a superposition of the flow created directly by the point force and the modifications to it, denoted as $\mathbf{u}^*(\mathbf{r})$, due to the surface of the sphere:

$$\mathbf{u}_a(\mathbf{r}) = -\mathbf{T}(\mathbf{r} \pm \ell\hat{\mathbf{n}})\cdot\mathbf{f}^{\rm sp} + \mathbf{u}^*(\mathbf{r}). \tag{7}$$

The field $\mathbf{u}^*(\mathbf{r})$ can effectively be ascribed to an image system of the point force created by the sphere [52]. It is given by the exact expression,

$$\begin{aligned}\mathbf{u}^*(\mathbf{r}) = {} & g_{a/\ell}\,\mathbf{f}^{\rm sp}\cdot\mathbf{T}(\mathbf{r} - \mathbf{r}^*) \\ & - h_{a/\ell}\,af^{\rm sp}\left[\left(\hat{\mathbf{n}}\hat{\mathbf{n}} - \tfrac{1}{3}\mathbf{I}\right)\cdot\nabla\right]\cdot\mathbf{T}(\mathbf{r} - \mathbf{r}^*) \\ & + j_{a/\ell}\,a^2\mathbf{f}^{\rm sp}\cdot\nabla^2\mathbf{T}(\mathbf{r} - \mathbf{r}^*),\end{aligned} \tag{8}$$

where $g_{a/\ell} = (3/2)[a/\ell - (a/\ell)^3/3]$ as defined earlier, $h_{a/\ell} = a^2/\ell^2 - a^4/\ell^4$, and $j_{a/\ell} = (1/4)(a/\ell)(1 - a^2/\ell^2)^2$. The point $\mathbf{r}^* = \mp\ell^*\hat{\mathbf{n}}$, with $\ell^* := a^2/\ell$ denotes the position of the image system of the point force $\mathbf{f}^{\rm spc}$ [52]; see Fig. 1(b).

The singularity solutions for the image system of the point force consist of a Stokeslet (point force), a stresslet, and a degenerate quadrupole (source dipole) with strengths $g_{a/\ell}$, $h_{a/\ell}$, and $2j_{a/\ell}a^2$, respectively [52]. We note that $\mathbf{u}_a(\mathbf{r}_S) = 0$ at any point $\mathbf{r}_S$ on the surface of the swimmer satisfying the no-slip boundary condition for a stationary sphere.

The flow field $\mathbf{u}_b$ set up by a sphere translating with the velocity $\mathbf{v}^{\rm sp}$ is obtained as [35]

$$\mathbf{u}_b(\mathbf{r}) = 8\pi\eta\left[\frac{3a}{4}\mathbf{T}(\mathbf{r}) + \frac{a^3}{8}\nabla^2\mathbf{T}(\mathbf{r})\right]\cdot\mathbf{v}^{\rm sp}, \tag{9}$$

where $\mathbf{v}^{\rm sp}$ is given by Eq. (6). Consequently, the total flow field of a spherical swimmer reads as

$$\begin{aligned}\mathbf{u}^{\rm sp}(\mathbf{r}) &= \mathbf{u}_a(\mathbf{r}) + \mathbf{u}_b(\mathbf{r})\\ &= \left\{(1-g_{a/\ell})\left[\mathbf{T}(\mathbf{r}) - \frac{a^2}{3}\widetilde{\mathbf{T}}(\mathbf{r})\right] - \mathbf{T}(\mathbf{r}\pm\ell\hat{\mathbf{n}})\right.\\ &\quad \left. + g_{a/\ell}\,\mathbf{T}(\mathbf{r}\pm\ell^*\hat{\mathbf{n}}) - 2j_{a/\ell}\,a^2\widetilde{\mathbf{T}}(\mathbf{r}\pm\ell^*\hat{\mathbf{n}})\right\}\cdot\mathbf{f}^{\rm sp}\\ &\quad + h_{a/\ell}\,a f^{\rm sp}\mathbf{H}(\mathbf{r}\pm\ell^*\hat{\mathbf{n}},\hat{\mathbf{n}})\cdot(\mathbf{r}\pm\ell^*\hat{\mathbf{n}}).\end{aligned} \tag{10}$$

Here the $+$ and $-$ signs apply to the pusher and puller types, respectively. For brevity, we have defined the new tensors, $\widetilde{\mathbf{T}}(\mathbf{r}) = -(1/2)\nabla^2\mathbf{T}(\mathbf{r}) = (1/8\pi\eta r^3)(-\mathbf{I} + 3\mathbf{rr}/r^2)$ and $\mathbf{H}(\mathbf{r},\hat{\mathbf{n}}) = (1/8\pi\eta r^3)[-\mathbf{I} + 3(\hat{\mathbf{n}}\cdot\mathbf{r})^2\mathbf{I}/r^2]$. Note that $\widetilde{\mathbf{T}}(\mathbf{r})\cdot\hat{\mathbf{n}}$ corresponds to the flow field of a degenerate quadrupole, and $\mathbf{H}(\mathbf{r},\hat{\mathbf{n}})\cdot\mathbf{r}$ gives the flow field of a force dipole oriented in the direction $\hat{\mathbf{n}}$. Since Eqs. (7)–(9) are exact, Eq. (10) represents the exact form of the flow field for our model swimmer valid at any distance r.

In Fig. 3 we have plotted the streamlines of the flow fields of a pusher and a puller respectively, described by Eq. (10), in a plane containing their orientation vectors $\hat{\mathbf{n}} = -\hat{\mathbf{x}}$. As expected, for a pusher (puller), there is an outward (inward) flow along the axis containing $\hat{\mathbf{n}}$ and an inward (outward) flow normal to that.

3. *Multipole expansion of the flow field*

Having obtained the full flow field of the microswimmer, we now investigate its far-field behavior. An axisymmetric rotation-free (no active torque) swimmer, with its body centered at the origin and self-propelling in the direction $\hat{\mathbf{n}}$ generates a far-field flow of the general form [53]

$$\begin{aligned}\mathbf{u}^{\rm sp}_{r\gg a}(\mathbf{r}) &= S^{\rm eff}(\hat{\mathbf{n}}\cdot\nabla)[\mathbf{T}(\mathbf{r})\cdot\hat{\mathbf{n}}]\\ &\quad - \frac{1}{2}D^{\rm eff}\nabla^2[\mathbf{T}(\mathbf{r})\cdot\hat{\mathbf{n}}]\\ &\quad + Q^{\rm eff}(\hat{\mathbf{n}}\cdot\nabla)^2[\mathbf{T}(\mathbf{r})\cdot\hat{\mathbf{n}}] + O(1/r^4).\end{aligned} \tag{11}$$

These terms describe the leading order singularity solutions of the Stokes equation for a force-free swimmer. They correspond to a force dipole, a degenerate quadrupole (source dipole), and a force quadrupole, respectively. The coefficients $S^{\rm eff}$, $D^{\rm eff}$, and $Q^{\rm eff}$ characterize the strengths of the respective multipoles and their values depend on the swimmer model under consideration. The flow filed of the force dipole decays as $1/r^2$ and those of the two quadrupolar terms as $1/r^3$. To obtain the multipolar strengths for our model, we expand $\mathbf{u}^{\rm sp}(\mathbf{r})$ given in Eq. (10) in powers of the inverse distance $1/r$ from the center of mass of the swimmer.

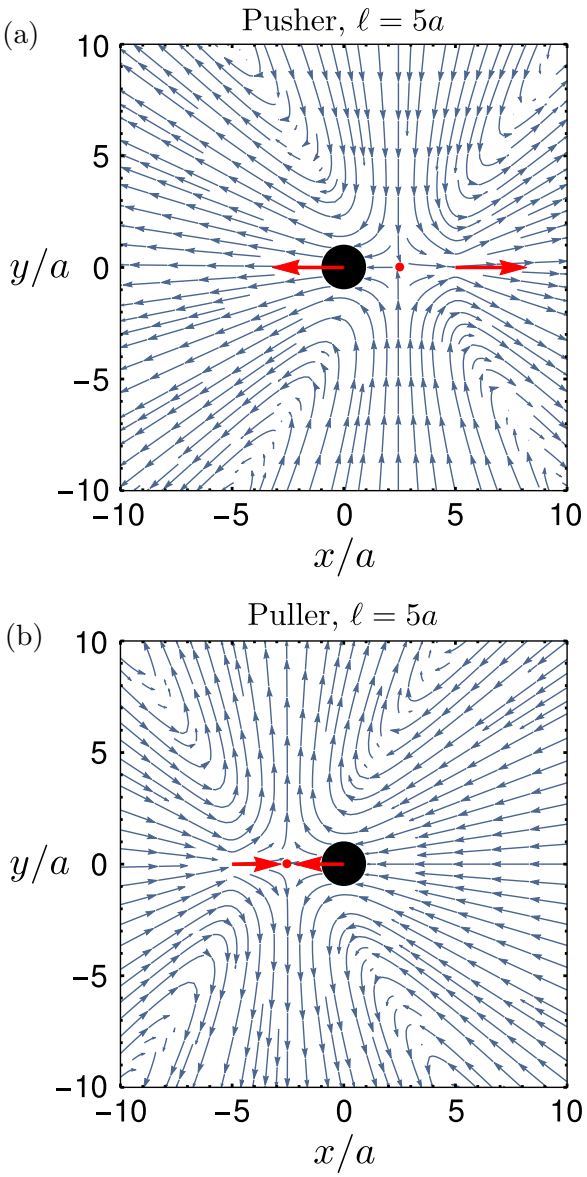

FIG. 3. The flow streamlines (blue arrows) created by a spherical swimmer of radius a, with orientation $\hat{\mathbf{n}} = -\hat{\mathbf{x}}$ and $\ell = 5a$, plotted in the x-y plane. Panels (a) and (b) correspond to a pusher and a puller type swimmer, respectively. The red arrows represent the active forces $\mathbf{f}^{\rm sp}$ and $\mathbf{f}^{\rm spc} = -\mathbf{f}^{\rm sp}$, and the red dot indicates the effective center $\mathbf{r}_c^{\rm eff}$ of the equivalent far-field point-force dipole in each case.

We find that for our model the first leading order term at far distances ($r \gg \ell > a$) decays as $1/r^2$ and is given by

$$\mathbf{u}^{\rm sp}_{r\gg\ell}(\mathbf{r}) = \pm\frac{1}{8\pi\eta}\frac{S^{\rm eff}}{r^2}[-1 + 3(\hat{\mathbf{r}}\cdot\hat{\mathbf{n}})^2]\hat{\mathbf{r}}. \tag{12}$$

It is identical to the flow field of a point-force dipole with an effective dipole strength

$$S^{\rm eff} = S^0[1 - (a/\ell)^2 g_{a/\ell} \pm (a/\ell)h_{a/\ell}], \tag{13}$$

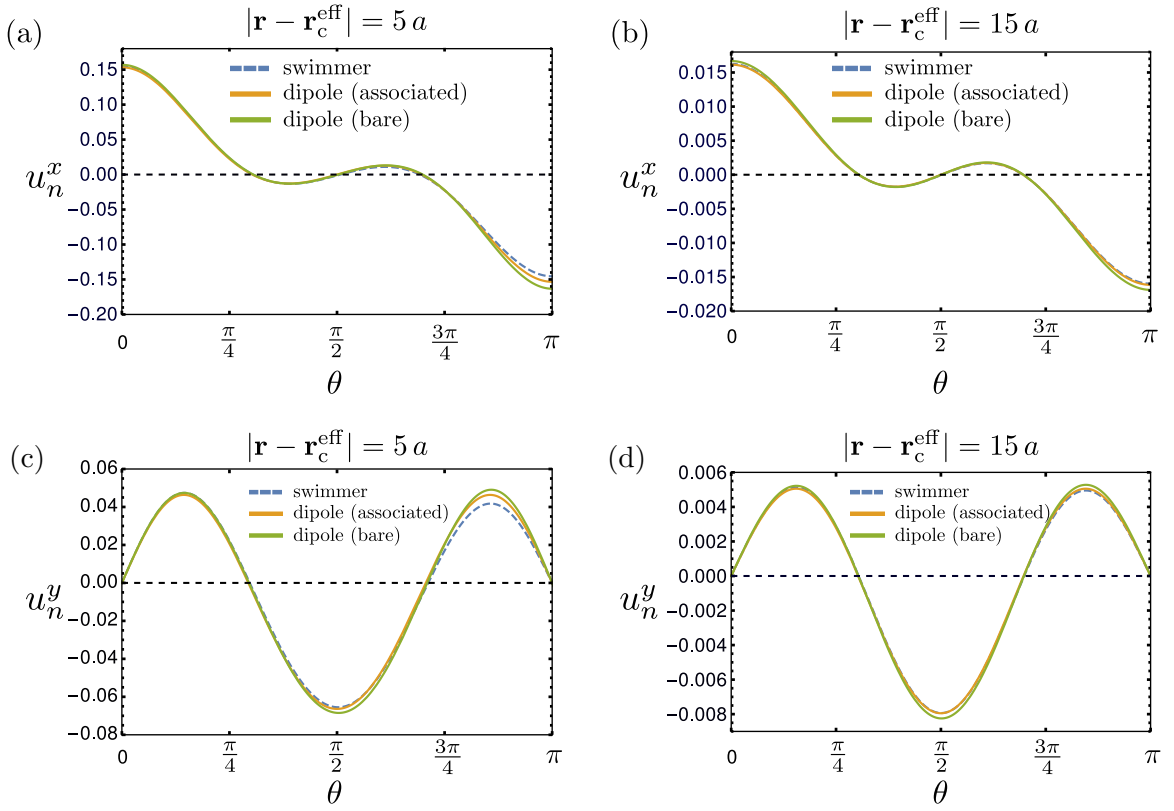

FIG. 4. Angular dependence of the flow fields of a swimmer with $\ell = 2.5a$ (pusher) and its associated point-force dipole and that of the bare point-force dipole obtained in the limit of zero swimmer size. For each case, the normalized flow field $u_{\rm n}^{\alpha}(|\mathbf{r}-\mathbf{r}_c^{\rm eff}|,\theta) = u^{\alpha}(|\mathbf{r}-\mathbf{r}_c^{\rm eff}|,\theta)/(f^{\rm sp}/6\pi\eta a)$ with $\alpha = x, y$, is shown as a function of the angle θ about the effective center $\mathbf{r}_c^{\rm eff}$ measured at distances $|\mathbf{r}-\mathbf{r}_c^{\rm eff}| = 5\,a$ [(a), (c)] and $15\,a$ [(b), (d)].

where $+$ and $-$ refer to a pusher and puller, respectively. Here $S^0 = \ell f^{\rm sp}$ represents the dipole strength of a point-force dipole consisting of two point forces of magnitude $f^{\rm sp}$ that lie at a distance ℓ apart. S^0 is identical to the *effective* dipole strength of the swimmer when $a/\ell \to 0$. However, for an accurate far-field representation of a finite-sized swimmer by a point-force dipole, the driving forces $f^{\rm sp}$ must be separated by an effective distance $\ell^{\rm eff} = \ell[1-(a/\ell)^2 g_{a/\ell} \pm (a/\ell)h_{a/\ell}] < \ell$. This implies that the effective center of the force, $-\oint_S dS'\,\mathbf{f}(\mathbf{r}'_S)$, on the fluid by the surface of the swimmer, or equivalently, the point of action of the force $\mathbf{f}^{\rm sp}$ on the swimmer, is situated at $-\hat{\mathbf{n}}(\ell-\ell^{\rm eff})$, which is slightly shifted from the center of mass $\mathbf{r}_{\rm cm}$ of the sphere. For clarity, *associated point-force dipole* is defined as the point-force dipole that consists of the two point forces $\pm\mathbf{f}^{\rm sp}$ separated by a distance $\ell^{\rm eff}$. The center of the *associated point-force dipole* lies at $\mathbf{r}_c^{\rm eff} = -\hat{\mathbf{n}}(\ell-\ell^{\rm eff}/2)$ (see Fig. 3). Similarly, by a *bare* point-force dipole we refer to the dipole obtained in the limit of $a/\ell \to 0$, where the two point forces are separated by a distance ℓ.

In the inset of Fig. 2, we have shown $S^{\rm eff}$ as a function of a/ℓ for both a pusher and a puller. We see that the effective dipole strength is renormalized differently for pushers and pullers. This difference results from the symmetry of the image stresslet [the term $\propto h_{a/\ell}$ in Eq. (8)], which always acts like a pusher. Thus, this term enhances the dipolar strength of a pusher, whereas it reduces that of a puller. Evidently, when $\ell \gg a$, the swimmer's size can be neglected and $S^{\rm eff} \to S^0$. Otherwise, even for the far-field flow, the finite size of the swimmer should be taken into account by renormalizing the dipole strength to $S^{\rm eff}$.

We depict the effect of such a renormalization on the flow field in Fig. 4. The figure shows the angular dependence of the normalized components of the flow field of a swimmer moving in $-\hat{\mathbf{x}}$ direction, i.e., $u_{\rm n}^{\alpha}(|\mathbf{r}-\mathbf{r}_c^{\rm eff}|,\theta) = u^{\alpha}(|\mathbf{r}-\mathbf{r}_c^{\rm eff}|,\theta)/(f^{\rm sp}/6\pi\eta a)$ where $\alpha = x, y$. For comparison, we have also included the corresponding flow fields of the associated and bare point-force dipoles. Here $|\mathbf{r}-\mathbf{r}_c^{\rm eff}|$ is the distance measured from the effective center $\mathbf{r}_c^{\rm eff}$ and θ is the angle between $\mathbf{r}-\mathbf{r}_c^{\rm eff}$ and $\hat{\mathbf{x}} = -\hat{\mathbf{n}}$ [Fig. 1(b)]. We find that at short distances [$r = 5a$ in Figs. 4(a) and 4(c)] there is a considerable difference between the flow fields of the swimmer and the bare point-force dipole, especially near $\theta = \pi$. However, the difference is reduced for the associated point-force dipole but still visible for the directions in front of the swimmer, especially for $\theta > 3\pi/4$. At farther distances, *e.g.*, at $r = 15a$, as presented in Figs. 4(b) and 4(d), we find a very good agreement between the flow fields of the swimmer and its associated point-force dipole, but they considerably differ from that of of the bare point-force dipole.

Subsequently, we obtain the coefficients of the next leading order terms ($\propto 1/r^3$). The strength of the degenerate quadrupolar term $\frac{1}{2}\hat{\mathbf{n}}\cdot\nabla^2\mathbf{T}(\mathbf{r})$ is given by

$$D^{\rm eff} = -[2j_{a/\ell} + (1-g_{a/\ell})/3]f^{\rm sp}a^2. \qquad (14)$$

$D^{\rm eff}$ is a function of both a and ℓ as it stems from the finite size of the cell body. The strength of the force quadrupolar term

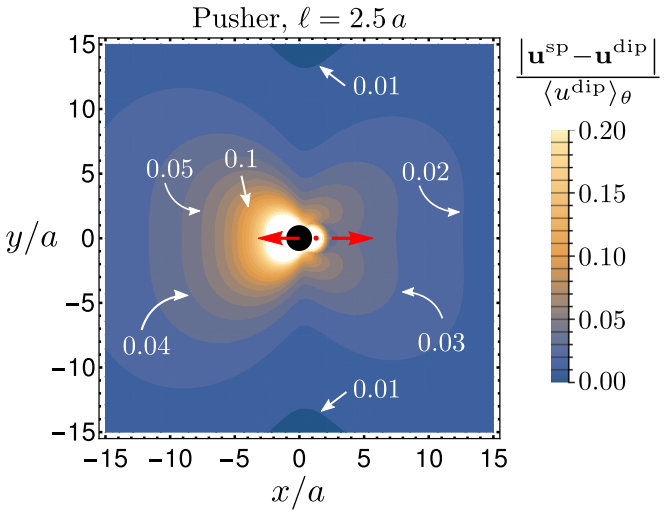

FIG. 5. Comparison of the flow fields of the swimmer with $\ell = 2.5a$ (pusher) and its associated point-force dipole. The figure shows the contour plot of the magnitude of the difference of the flows of the swimmer and its associated point-force dipole, $|\mathbf{u}^{sp}(\mathbf{r}) - \mathbf{u}^{dip}(\mathbf{r})|$, normalized by the angular averaged flow speed of the dipole, $\langle u^{dip}(|\mathbf{r} - \mathbf{r}_c^{eff}|)\rangle_\theta$, at the corresponding distance from the center $\mathbf{r}_c^{eff}$. The body of the swimmer is shown in black; the active forces $\mathbf{f}^{sp}$ and $\mathbf{f}^{spc}$ and the effective center $\mathbf{r}_c^{eff}$ of the associated point-force dipole are shown in red. The white region (lighter color) represents values in the range 0.2–0.8 not shown in the color bar.

$(\hat{\mathbf{n}}\cdot\nabla)^2\mathbf{T}(\mathbf{r})$ is given by

$$Q^{eff} = -[1 - g_{a/\ell}(a/\ell)^4 \pm (a/\ell)^3 h_{a/\ell}] f^{sp}\ell^2. \quad (15)$$

Q^{eff} results from the length asymmetry between size of the cell body a and the effective length of the flagellum ℓ [53]. Note that unlike the dipolar strength, the quadrupolar strengths have the dimension of force times length squared and they vanish for a pointlike swimmer, i.e., $a \to 0$ and $\ell \to 0$, such that $S^0 = \ell f^{sp}$ remains constant.

4. *Swimmer's finite-size effects on the flow field*

Next, we examine the flow field at intermediate distances more closely and compare it to that of a point-force dipole. For simplicity we focus on the x-y plane. In the following, $\mathbf{u}^{sp}$ and $\mathbf{u}^{dip}$ denote the swimmer's flow field and that of its associated point-force dipole with the strength S^{eff} respectively. In Fig. 5 we have presented the contour plot of the difference of the two flow fields, $|\mathbf{u}^{sp}(\mathbf{r}) - \mathbf{u}^{dip}(\mathbf{r})|$ normalized by the angular averaged flow speed of the dipole, $\langle u^{dip}(|\mathbf{r} - \mathbf{r}_c^{eff}|)\rangle_\theta$, for a pusher with $\ell = 2.5a$.

From Fig. 5 we notice that the angular dependence of the swimmer's flow field at intermediate distances is significantly different from that of a point-force dipole. In particular, the front-back symmetry of the flow field of a point-force dipole is broken by the finite size of the swimmer's body. This dissimilarity is visible in the head-tail asymmetry of the shapes of the contours around the swimmer. For example, the contour for 0.05 (5% difference in the flow speeds) extends up to a distance of $\sim 8a$ from $\mathbf{r}_c^{eff}$ towards the head, whereas, at similar distances towards the back, the normalized difference is < 0.03 (i.e., $< 3\%$). Furthermore, contours of any given normalized difference encircle a larger area in the front than in the back. Hence, the flow field of the swimmer approaches that of the dipole at a shorter distance in any general direction behind the swimmer (i.e., for $\theta < \pi/2$), while at the same distance in a corresponding direction in the front (i.e., for $\theta + \pi/2$), we notice remarkable differences, in agreement with our observations from Fig. 4.

The differences between the flow field of the swimmer and that of its associated force dipole with the same strength reflect the importance of the next leading order singularity contributions (quadrupolar, octoupolar, etc.) to the flow field at short and intermediate distances. These higher order singularity contributions are important for the collective behavior of the microwswimmers and need to be accounted for in the many-body simulations.

C. Dynamics of a swimmer exposed to external forces and torques

An external force acting on a swimmer supplements to its self-propulsion velocity $\mathbf{v}^{sp}$. Similarly, an external torque $\mathbf{L}^{ext}$ causes the swimmer to rotate. Note that the flow created by self-propulsion of the swimmer does not generate any angular velocity in the absence of other swimmers [50]. Thus, the translational and angular velocities of the swimmer in the presence of the external force $\mathbf{f}^{ext}$ and torque $\mathbf{L}^{ext}$ are modified as

$$\mathbf{v} = \mathbf{v}^{sp} + \frac{1}{6\pi\eta a}\mathbf{f}^{ext}, \quad (16)$$

$$\boldsymbol{\omega} = \frac{1}{8\pi\eta a^3}\mathbf{L}^{ext}. \quad (17)$$

The flow field $\mathbf{u}_b(\mathbf{r})$ resulting from the translation of the sphere is accordingly altered. The contribution of the external force to the flow can be obtained by substituting $\mathbf{v}^{sp}$ with $\frac{1}{6\pi\eta a}\mathbf{f}^{ext}$ in Eq. (9). Likewise, the rotation of the swimmer generates a flow field which is described by $(a^3/r^3)\boldsymbol{\omega}\times\mathbf{r}$ [35]. Given the linearity of Stokes equation, the net flow field of the swimmer in the presence of external forces and torques is thus given by

$$\mathbf{u}(\mathbf{r}) = \mathbf{u}^{sp}(\mathbf{r}) + \left[\mathbf{T}(\mathbf{r}) + \frac{a^2}{6}\nabla^2\mathbf{T}(\mathbf{r})\right]\cdot\mathbf{f}^{ext} + \frac{1}{8\pi\eta r^3}\mathbf{L}^{ext}\times\mathbf{r}. \quad (18)$$

in which the $\mathbf{u}^{sp}(\mathbf{r})$ is obtained from Eq. (10).

Having discussed the motion of a single swimmer, we devote the next section to the hydrodynamic interactions among an ensemble of swimmers in a suspension.

III. HYDRODYNAMIC INTERACTIONS AMONG SPHERICAL SWIMMERS

In a suspension of N swimmers, the flow field generated by each swimmer will affect the motion of all the others. In this section, we obtain the grand mobility tensor that connects the translational and angular velocities of the swimmers to the forces and torques acting on them. Especially, we elucidate the contribution of the active forces to hydrodynamic interactions.

The translational velocity $\mathbf{v}_i$ and angular velocity $\boldsymbol{\omega}_i$ of the ith swimmer are coupled to the forces and torques acting on

all the swimmers via the grand mobility tensors defined as

$$\begin{bmatrix}\mathbf{v}_i\\ \boldsymbol{\omega}_i\end{bmatrix} = \sum_{j=1}^{N}\begin{bmatrix}\mathbf{M}^{\mathrm{tt}}_{ij} & \mathbf{M}^{\mathrm{tr}}_{ij}\\ \mathbf{M}^{\mathrm{rt}}_{ij} & \mathbf{M}^{\mathrm{rr}}_{ij}\end{bmatrix}\begin{bmatrix}\mathbf{f}^{\mathrm{ext}}_j\\ \mathbf{L}^{\mathrm{ext}}_j\end{bmatrix} + \sum_{j=1}^{N}\begin{bmatrix}\boldsymbol{\mu}^{\mathrm{tt}}_{ij} & \boldsymbol{\mu}^{\mathrm{tr}}_{ij}\\ \boldsymbol{\mu}^{\mathrm{rt}}_{ij} & \boldsymbol{\mu}^{\mathrm{rr}}_{ij}\end{bmatrix}\begin{bmatrix}\mathbf{f}^{\mathrm{sp}}_j\\ \mathbf{0}\end{bmatrix}. \tag{19}$$

Here the subscripts i, j are the swimmer indices running from 1 to N, and the superscripts t and r stand for "translational" and "rotational" degrees of freedom, respectively. The mobility tensors $\mathbf{M}^{\alpha\beta}_{ij}$ couple the ith swimmer's translational and angular velocities (specified by the index α) to the passive external forces $\mathbf{f}^{\mathrm{ext}}_j$ and torques $\mathbf{L}^{\mathrm{ext}}_j$ (distinguished by the index β) acting on the jth swimmer. Accordingly, the tensors $\mathbf{M}$ are identical to the corresponding mobilities of passive spheres. In contrast, the active mobility tensors $\boldsymbol{\mu}$ incorporate the hydrodynamic interactions resulting from the active forces. They couple the velocities of the ith swimmer to the active forces $\pm\mathbf{f}^{\mathrm{sp}}_j$ that propel the jth swimmer. Below, we calculate the explicit forms of the $\boldsymbol{\mu}$ tensors for this model system.

A. Self-mobility tensors

We first focus on the self-mobility tensors. $\mathbf{M}^{\mathrm{tt}}_{ii}$ and $\mathbf{M}^{\mathrm{rr}}_{ii}$ represent, respectively, the translational and rotational self-mobility tensors of the ith sphere in the absence of self-propulsion [35]. $\boldsymbol{\mu}^{\mathrm{tt}}_{ii}$ and $\boldsymbol{\mu}^{\mathrm{rr}}_{ii}$ denote the corresponding active self-mobility tensors. To simplify the notation, in what follows, we introduce the following abbreviations:

$$M^{\mathrm{t}} = \frac{1}{6\pi\eta a}, \quad M^{\mathrm{r}} = \frac{1}{8\pi\eta a^3}, \quad \mu^{\mathrm{t}} = \frac{1-g_{a/\ell}}{6\pi\eta a}. \tag{20}$$

The passive translational and rotational mobility tensors of the spheres follow from Eqs. (16) and (17), and they read as $\mathbf{M}^{\mathrm{tt}}_{ii} = M^{\mathrm{t}}\mathbf{I}, \mathbf{M}^{\mathrm{rr}}_{ii} = M^{\mathrm{r}}\mathbf{I}$. Furthermore, for spheres, we have $\mathbf{M}^{\mathrm{tr}}_{ii} = \mathbf{M}^{\mathrm{rt}}_{ii} = \mathbf{0}$ [35]. Likewise, we can read off the active mobility tensors from Eq. (6) as $\boldsymbol{\mu}^{\mathrm{tt}}_{ii} = \mu^{\mathrm{t}}\mathbf{I}$ and from Eq. (17) as $\boldsymbol{\mu}^{\mathrm{rt}}_{ii} = \mathbf{0}$. The remaining active self-mobilities, $\boldsymbol{\mu}^{\mathrm{rr}}_{ii}$ and $\boldsymbol{\mu}^{\mathrm{tr}}_{ii}$, are irrelevant to the dynamics as the presented model does not include any active torques.

B. Cross-mobility tensors

We now discuss the cross-mobility tensors $\mathbf{M}^{\alpha\beta}_{ij}$ and $\boldsymbol{\mu}^{\alpha\beta}_{ij}$ for $i \neq j$ that result from the interactions between two distinct swimmers i and j. In particular, we derive the form of $\boldsymbol{\mu}^{\alpha\beta}_{ij}$ tensors. To obtain the explicit form of the hydrodynamic interactions between the swimmers, we exploit the Faxen's theorems [35].

The Faxen's theorems relate the translational and angular velocities of a sphere to the forces, torques and external flows imposed on it. Hence, the translational and rotational velocities of the ith swimmer in the flow generated by the motion of all the other swimmers are given by

$$\mathbf{v}_i = M^{\mathrm{t}}\mathbf{f}^{\mathrm{ext}}_i + \mu^{\mathrm{t}}\mathbf{f}^{\mathrm{sp}}_i + \left(1+\frac{a^2}{6}\nabla^2_{r_i}\right)\sum_{j\neq i}\mathbf{u}_j(\mathbf{r}_i), \tag{21}$$

$$\boldsymbol{\omega}_i = M^{\mathrm{r}}\mathbf{L}^{\mathrm{ext}}_i + \frac{1}{2}\boldsymbol{\nabla}_{r_i}\times\sum_{j\neq i}\mathbf{u}_j(\mathbf{r}_i), \tag{22}$$

where $\sum_{j\neq i}\mathbf{u}_j(\mathbf{r}_i)$ is the total flow field in the absence of the ith swimmer at its center $\mathbf{r}_i$ created by all the other swimmers. Substituting the explicit form of $\mathbf{u}_j(\mathbf{r}_i)$ from Eq. (18) in the above equations provides us with the mobility tensors $\mathbf{M}^{\alpha\beta}_{ij}$ for $i \neq j$ [35]:

$$\mathbf{M}^{\mathrm{tt}}_{ij} = M^{\mathrm{t}}\left[\frac{3a}{4r_{ij}}(\mathbf{I}+\hat{\mathbf{r}}_{ij}\hat{\mathbf{r}}_{ij}) + \frac{1}{2}\left(\frac{a}{r_{ij}}\right)^3(\mathbf{I}-3\hat{\mathbf{r}}_{ij}\hat{\mathbf{r}}_{ij})\right] \equiv \mathbf{M}^{\mathrm{tt}}(\mathbf{r}_{ij}), \tag{23}$$

$$\mathbf{M}^{\mathrm{rr}}_{ij} = -M^{\mathrm{r}}\frac{1}{2}\left(\frac{a}{r_{ij}}\right)^3(\mathbf{I}-3\hat{\mathbf{r}}_{ij}\hat{\mathbf{r}}_{ij}) \equiv \mathbf{M}^{\mathrm{rr}}(\mathbf{r}_{ij}), \tag{24}$$

$$\mathbf{M}^{\mathrm{tr}}_{ij} = \mathbf{M}^{\mathrm{rt}}_{ij} = M^{\mathrm{r}}a\left(\frac{a}{r_{ij}}\right)^2\hat{\mathbf{r}}_{ij}\times \equiv \mathbf{M}^{\mathrm{tr}}(\mathbf{r}_{ij})\times, \tag{25}$$

in which $\mathbf{r}_{ij} := \mathbf{r}_i - \mathbf{r}_j$ and $r_{ij} := |\mathbf{r}_{ij}|$ and the expressions are correct up to the order $(a/r_{ij})^3$. The tensor $\mathbf{M}^{\mathrm{tt}}_{ij}$ given above is the well-known Rotne-Prager mobility tensor for passive spheres. Note that, here and below, whenever the operator '$\times$' appears at the end of a tensor (*e.g.*, in $\mathbf{M}^{\mathrm{tr}}_{ij}$), it is understood that a cross product should be taken with the appropriate right-hand operand [given by the conventional matrix multiplication of Eq. (19)].

In a similar manner, we derive the active mobility tensors $\boldsymbol{\mu}^{\alpha\beta}_{i\neq j}$ correct up to the order $(a/r_{ij})^3$ as given below:

$$\boldsymbol{\mu}^{\mathrm{tt}}_{ij} = \boldsymbol{\mu}^{\mathrm{tt}}_0(\mathbf{r}_{ij}) + \boldsymbol{\mu}^{\mathrm{tt}}_{\ell}(\mathbf{r}^{\ell}_{ij}) + \boldsymbol{\mu}^{\mathrm{tt}}_{\ell^*}(\mathbf{r}^{\ell^*}_{ij}), \tag{26}$$

$$\boldsymbol{\mu}^{\mathrm{rt}}_{ij} = \boldsymbol{\mu}^{\mathrm{rt}}_0(\mathbf{r}_{ij}) + \boldsymbol{\mu}^{\mathrm{rt}}_{\ell}(\mathbf{r}^{\ell}_{ij}) + \boldsymbol{\mu}^{\mathrm{rt}}_{\ell^*}(\mathbf{r}^{\ell^*}_{ij}), \tag{27}$$

where $\mathbf{r}^{\ell}_{ij} := \mathbf{r}_{ij} \pm \ell\hat{\mathbf{n}}_j$, $\mathbf{r}^{\ell^*}_{ij} := \mathbf{r}_{ij} \pm \ell^*\hat{\mathbf{n}}_j$. The functions appearing on the right-hand sides are given by

$$\boldsymbol{\mu}^{\mathrm{tt}}_0(\mathbf{r}) = (1-g_{a/\ell})\mathbf{M}^{\mathrm{tt}}(\mathbf{r}), \tag{28}$$

$$\boldsymbol{\mu}^{\mathrm{tt}}_{\ell}(\mathbf{r}) = -M^{\mathrm{t}}\left[\frac{3a}{4r}(\mathbf{I}+\hat{\mathbf{r}}\hat{\mathbf{r}}) + \frac{1}{4}\left(\frac{a}{r}\right)^3(\mathbf{I}-3\hat{\mathbf{r}}\hat{\mathbf{r}})\right], \tag{29}$$

$$\boldsymbol{\mu}^{\mathrm{tt}}_{\ell^*}(\mathbf{r}) = -g_{a/\ell}\,\boldsymbol{\mu}^{\mathrm{tt}}_{\ell}(\mathbf{r}) + 2j_{a/\ell}M^{\mathrm{t}}\frac{3}{4}\left(\frac{a}{r}\right)^3(\mathbf{I}-3\hat{\mathbf{r}}\hat{\mathbf{r}}) + h_{a/\ell}[-\hat{\mathbf{r}}+3(\hat{\mathbf{r}}\cdot\hat{\mathbf{n}}_j)^2\hat{\mathbf{r}}]M^{\mathrm{t}}\frac{3}{4}\left(\frac{a}{r}\right)^2\hat{\mathbf{n}}_j, \tag{30}$$

$$\boldsymbol{\mu}^{\mathrm{rt}}_0(\mathbf{r}) = (1-g_{a/\ell})\frac{1}{8\pi\eta}\frac{\mathbf{r}}{r^3}\times, \tag{31}$$

$$\boldsymbol{\mu}^{\mathrm{rt}}_{\ell}(\mathbf{r}) = -\frac{1}{8\pi\eta}\frac{\mathbf{r}}{r^3}\times, \tag{32}$$

$$\boldsymbol{\mu}^{\mathrm{rt}}_{\ell^*}(\mathbf{r}) = 3h_{a/\ell}\frac{\hat{\mathbf{n}}_j\cdot\mathbf{r}(\hat{\mathbf{n}}_j\times\mathbf{r})\hat{\mathbf{n}}_j}{8\pi\eta r^5} + g_{a/\ell}\frac{1}{8\pi\eta}\frac{\mathbf{r}}{r^3}\times. \tag{33}$$

In the limit $a/\ell \to 0$, we recover the active mobility tensors of a bare point-force dipole:

$$\boldsymbol{\mu}^{\mathrm{tt}}_{ij} = (1/8\pi\eta)\left[(\mathbf{I}+\hat{\mathbf{r}}_{ij}\hat{\mathbf{r}}_{ij})/r_{ij} - \left(\mathbf{I}+\hat{\mathbf{r}}^{\ell}_{ij}\hat{\mathbf{r}}^{\ell}_{ij}\right)/r^{\ell}_{ij}\right], \tag{34}$$

$$\boldsymbol{\mu}^{\mathrm{rt}}_{ij} = (1/8\pi\eta)[\mathbf{r}_{ij}/r^3_{ij} - \mathbf{r}^{\ell}_{ij}/(r^{\ell}_{ij})^3]\times. \tag{35}$$

The presented swimmer model does not include any active torques. Thus, the remaining active cross-mobilities $\boldsymbol{\mu}^{\mathrm{tr}}_{ij}$ and

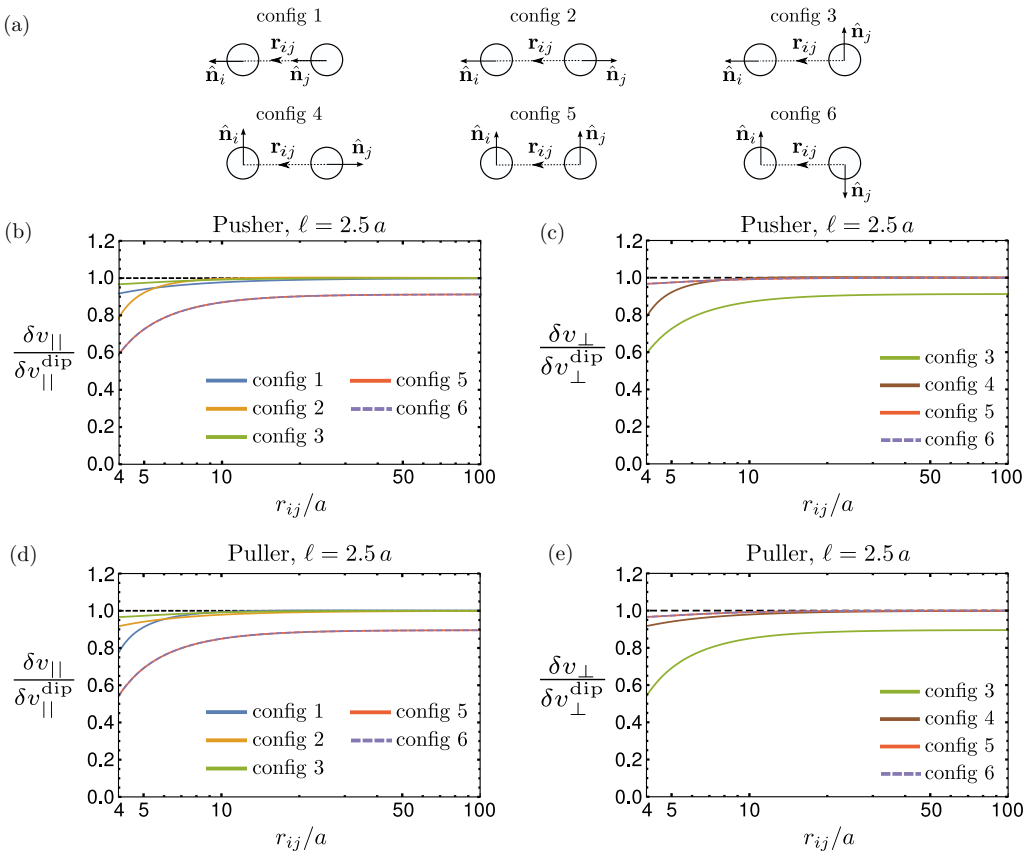

FIG. 6. The effect of the finite size of the swimmers on hydrodynamic interactions. (a) Schematics of six configurations for two swimmers i, j with respective orientations $\hat{\mathbf{n}}_i, \hat{\mathbf{n}}_j$ and a separation vector $\mathbf{r}_{ij}$. (b)–(e) The ratios $\delta v_{||}/\delta v_{||}^{\rm dip}$ and $\delta v_{\perp}/\delta v_{\perp}^{\rm dip}$ plotted as functions of the separation r_{ij}/a for $\ell = 2.5a$. Here $\delta v_{||}$ ($\delta v_{\perp}$) is the velocity increment in the direction parallel (perpendicular) to the orientation of a swimmer resulting from its hydrodynamic interactions with another swimmer. Similarly, $\delta v_{||}^{\rm dip}$ ($\delta v_{\perp}^{\rm dip}$) is the value for the corresponding associated point-force dipoles.

$\boldsymbol{\mu}_{ij}^{\rm rr}$ are irrelevant for the description of the dynamics. Note that unlike the passive mobility tensors, the active contributions depend on the swimmers' orientations. In the next subsection, we will discuss the consequences of active forces on the hydrodynamic interactions for finite-sized swimmers.

C. Activity-induced hydrodynamic interactions

We end our results with a preliminary examination of the consequences of active forces on the hydrodynamic interactions, and we will pay special attention to the consequences of the swimmer's finite size. For this purpose, we consider the velocity increment $\delta\mathbf{v}_i = \boldsymbol{\mu}_{ij}^{\rm tt} \cdot \mathbf{f}_j^{\rm sp}$ induced on the swimmer i due to the active forces $\pm\mathbf{f}_j^{\rm sp}$ of the swimmer j. Let $\delta v_{||}$ and $\delta v_{\perp}$ be the magnitudes of this velocity along and normal to $\mathbf{n}_i$, respectively. Likewise, we denote the corresponding speeds for an associated point-force dipole of strength $S^{\rm eff}$ as $\delta v_{||}^{\rm dip}$ and $\delta v_{\perp}^{\rm dip}$, respectively. They result from the interaction between the two corresponding associated point-force dipoles. Their values are obtained by using the mobility tensor given in Eq. (34) evaluated for $\mathbf{r}_{ij} \to \mathbf{r}_{ij} + (\ell - \ell^{\rm eff})\hat{\mathbf{n}}_j$ (with the transformation applied to the first term alone).

In Fig. 6 we show the ratios $\delta v_{||}/\delta v_{||}^{\rm dip}$ and $\delta v_{\perp}/\delta v_{\perp}^{\rm dip}$ as a function of the swimmer distance r_{ij} for $\ell = 2.5a$ for a few typical configurations of the swimmers i and j depicted schematically in Fig. 6(a). We observe that for the configurations 5 and 6, $\delta v_{||}/\delta v_{||}^{\rm dip}$ depicted in Figs. 6(b) and 6(d) and for the configuration 3, $\delta v_{\perp}/\delta v_{\perp}^{\rm dip}$ presented in Figs. 6(c) and 6(e) do not converge to unity even at very large distances. For all other configurations, the ratios go to unity for $r_{ij} > 20a$ as one would expect.

The disagreement between the activity-induced velocity increments of a finite-sized swimmer and that of a dipolar swimmer for some of the configurations can be understood as follows. The far-distance expansion of the mobility tensor for the swimmer yields to

$$\delta\mathbf{v}^{sp}(\mathbf{r}_{ij}) \equiv \boldsymbol{\mu}_{ij}^{\rm tt} \cdot \mathbf{f}_j^{\rm sp} = \frac{1}{8\pi\eta}\frac{S^{\rm eff}}{r_{ij}^2}[-1 + 3(\hat{\mathbf{r}}_{ij} \cdot \hat{\mathbf{n}})^2]\hat{\mathbf{r}}_{ij} + O\left(\frac{1}{r_{ij}^3}\right). \quad (36)$$

As expected, the leading order term above is identical to the corresponding leading order term of the mobility tensor of the associated force dipole that is centered at $\mathbf{r}_{ij} + (\ell - \ell_{\rm eff}/2)\hat{\mathbf{n}}_j$. However, the coefficients of the next leading order term $O(\frac{1}{r_{ij}^3})$ for the swimmer is different from that for the associated dipole.

We note that the leading order term in Eq. (36) is always along $\hat{\mathbf{r}}_{ij}$. For the specific configurations 5 and 6, $\hat{\mathbf{n}}_i \perp \hat{\mathbf{r}}_{ij}$. Hence, the velocity increment parallel to $\hat{\mathbf{n}}_i$ is determined by

the next leading order term ($\propto 1/r_{ij}^3$) that differs from that of the force dipoles. Thus, the ratios $\delta v_{||}/\delta v_{||}^{\rm dip}$ for configurations 5 and 6 of Figs. 6(b) and 6(d) do not converge to unity. Similarly, for the configuration 3, the velocity increment, $\delta v_\perp$, perpendicular to $\hat{\mathbf{n}}_i$ is normal to $\hat{\mathbf{r}}_{ij}$, and its value is determined by the $O(1/r_{ij}^3)$ term that is different from that of the dipoles. Therefore, $\delta v_\perp/\delta v_\perp^{\rm dip}$ of the configuration 3 presented in Figs. 6(c) and 6(e) also do not converge to unity. These observations highlight the importance of the swimmers' finite size for their hydrodynamic interactions. In our preliminary analysis, we have investigated only a few representative configurations. In a suspension, the difference in the velocity increments $\delta\mathbf{v}$ and $\delta\mathbf{v}^{\rm dip}$ in general depends on the relative orientations of the two swimmers with respect to their interconnecting line.

IV. CONCLUSIONS

We have investigated the finite body-size effects on the flow properties and hydrodynamic interactions of microswimmers by considering a minimal model for rigid-bodied microswimmers. Notably, we have investigated the consequences of the extended surface of the microswimmer on the interplay between its self-propulsion and flow properties. The model parameters include the body size a and the distance ℓ between the center of the body and the point of application of the thrust $-\mathbf{f}^{\rm sp}$ on the fluid. The presented model has important differences with the squirmer model for microswimmers [27,54,55]. The latter applies to swimmers with deformable surfaces. Moreover, in contrast to the squirmer model, the finite body size and self-propulsion in this model present two separate length scales a and ℓ intrinsic to each individual. As a result, the flow field of this model at a separation r crucially depends on both ℓ/r and a/ℓ.

We have calculated the swimmer's self-propulsion velocity and flow field as a function of a/ℓ. Our analysis shows that the behavior of the minimal swimmer deviates significantly from that of a point-force dipole unless $a/\ell \to 0$. The far-field flow of the swimmer can be mapped to that of a point-force dipole with an effective dipolar strength given by $S^{\rm eff} = f^{\rm sp}\ell^{\rm eff}$ where $\ell^{\rm eff}$ is smaller than ℓ. Thus, we have demonstrated that a point-force dipole can provide a relatively good description of the far filed behavior of a finite-sized spherical swimmer provided that we use $\ell^{\rm eff} = \ell^{\rm eff}(\ell,a)$ as the effective distance between the two point forces.

At intermediate distances, the flow field presents a remarkably different angular dependency in comparison to that of a force dipole due to the contribution of higher order multipoles. Furthermore, the finite body size breaks the inherent front-back symmetry of the flow field of dipolar swimmers. Therefore, the model naturally incorporates the head-tail asymmetry at the hydrodynamic interaction level that is an intrinsic feature of many microswimmers. These results highlight the necessity for the inclusion of the finite body size in simulations of microswimmer suspensions at moderate concentrations.

To investigate the finite body-size effects on hydrodynamic interactions and on the collective dynamics of the swimmers, we have derived the grand mobility tensor for the presented model. A preliminary investigation demonstrates that the finite body size significantly affects the strength of hydrodynamic interactions. The consequences of the finite body size and particularly the head-tail asymmetry of the flow field on the collective dynamics of swimmers is not yet probed. The collective behavior of minimal spherical swimmers can be investigated by Stokesian dynamics simulations and will be a subject of a future study. The mobility matrix elements describe long-range interactions and have rather cumbersome forms. Nevertheless, they can be properly decomposed by an Ewald summation technique to account for the long range of hydrodynamic interactions in numerical simulations [56].

To summarize, our model captures the essential features of microswimmers with finite-body size in a minimal fashion. It opens the door for exploring collective behavior of microswimmers at intermediate concentrations where point-force dipole approximation fails. The presented model is general, and it can be used to model microwswimmers that have a rigid body with flexible propelling appendage by a suitable choice of parameters.

ACKNOWLEDGMENTS

We are grateful to J. F. Brady for insightful discussions, the two unanimous referees for their very helpful comments, and we acknowledge financial support from the German Science Foundation (http://www.dfg.de) within SFB TRR 146 (project C6) (http://trr146.de).

[1] E. Lauga and T. R. Powers, Rep. Prog. Phys. **72**, 096601 (2009).
[2] J. Dunkel, S. Heidenreich, K. Drescher, H. H. Wensink, M. Bär, and R. E. Goldstein, Phys. Rev. Lett. **110**, 228102 (2013).
[3] S. Zhou, A. Sokolov, O. D. Lavrentovich, and I. S. Aranson, Proc. Natl. Acad. Sci. USA **111**, 1265 (2013).
[4] H. M. López, J. Gachelin, C. Douarche, H. Auradou, and E. Clément, Phys. Rev. Lett. **115**, 028301 (2015).
[5] R. R. Trivedi, R. Maeda, N. L. Abbott, S. E. Spagnolie, and D. B. Weibel, Soft Matter **11**, 8404 (2015).
[6] P. C. Mushenheim, R. R. Trivedi, H. H. Tuson, D. B. Weibel, and N. L. Abbott, Soft Matter **10**, 88 (2014).
[7] T. C. Adhyapak and H. Stark, Phys. Rev. E **92**, 052701 (2015).
[8] R. Vogel and H. Stark, Phys. Rev. Lett. **110**, 158104 (2013).
[9] P. J. A. Janssen and M. D. Graham, Phys. Rev. E **84**, 011910 (2011).
[10] S. Y. Reigh, R. G. Winkler, and G. Gompper, Soft Matter **8**, 4363 (2012).
[11] J. Saragosti, V. Calvez, N. Bournaveas, B. Perthame, A. Buguin, and P. Silberzan, Proc. Natl. Acad. Sci. USA **108**, 16235 (2011).
[12] S. P. Strong, B. Freedman, W. Bialek, and R. Koberle, Phys. Rev. E **57**, 4604 (1998).
[13] N. C. Darnton, L. Turner, S. Rojevsky, and H. C. Berg, J. Bacteriol. **189**, 1756 (2007).
[14] H. Wada and R. R. Netz, Europhys. Lett. **82**, 28001 (2008).

[15] O. Pohl, M. Hintsche, Z. Alirezaeizanjani, M. Seyrich, C. Beta, and H. Stark, PLoS Comput. Biol. **13**, e1005329 (2017).
[16] M. Kong, Y. Wu, G. Li, and R. G. Larson, Soft Matter **11**, 1572 (2015).
[17] S. Rafaï, L. Jibuti, and P. Peyla, Phys. Rev. Lett. **104**, 098102 (2010).
[18] B. M. Friedrich and F. Jülicher, Phys. Rev. Lett. **109**, 138102 (2012).
[19] I. H. Riedel, K. Kruse, and J. Howard, Science **309**, 300 (2005).
[20] G. Li and J. X. Tang, Phys. Rev. Lett. **103**, 078101 (2009).
[21] J. Elgeti and G. Gompper, Proc. Natl. Acad. Sci. USA **110**, 4470 (2013).
[22] D. Alizadehrad, T. Krüger, M. Engstler, and H. Stark, PLoS Comput. Biol. **11**, e1003967 (2015).
[23] R. Dreyfus, J. Baudry, M. Roper, H. Stone, M. Fermigier, and J. Bibette, Nature (London) **437**, 862 (2005).
[24] A. Ghosh and P. Fischer, Nano Lett. **9**, 2243 (2009).
[25] L. Zhang, J. J. Abbott, L. Dong, B. E. Kratochvil, D. Bell, and B. J. Nelson, Appl. Phys. Lett. **94**, 064107 (2009).
[26] M. C. Marchetti, J. F. Joanny, S. Ramaswamy, T. B. Liverpool, J. Prost, M. Rao, and R. A. Simha, Rev. Mod. Phys. **85**, 1143 (2013).
[27] M. Lighthill, Commun. Pure Appl. Math. **5**, 109 (1952).
[28] S. V. Srigiriraju and T. R. Powers, Phys. Rev. Lett. **94**, 248101 (2005).
[29] S. E. Spagnolie and E. Lauga, Phys. Rev. Lett. **106**, 058103 (2011).
[30] E. Lauga, Annu. Rev. Fluid Mech. **48**, 105 (2016).
[31] T. C. Adhyapak and H. Stark, Soft Matter **12**, 5621 (2016).
[32] H. H. Wensink, J. Dunkel, S. Heidenreich, K. Drescher, R. E. Goldstein, H. Löwen, and J. M. Yeomans, Proc. Natl. Acad. Sci. USA **109**, 14308 (2012).
[33] H. C. Fu, T. R. Powers, R. Stocker, *et al.*, Proc. Natl. Acad. Sci. USA **109**, 4780 (2012).
[34] A. Zöttl and H. Stark, Phys. Rev. Lett. **112**, 118101 (2014).
[35] J. Dhont, *An Introduction to Dynamics of Colloids* (Elsevier Science, Amsterdam, 1996).
[36] S. Kim and S. Karilla, *Microhydrodynamics: Principles and Selected Applications* (Dover Publications, New York, 2005).
[37] J. P. Hernandez-Ortiz, C. G. Stoltz, and M. D. Graham, Phys. Rev. Lett. **95**, 204501 (2005).
[38] Y. Fily, A. Baskaran, and M. C. Marchetti, Soft Matter **8**, 3002 (2012).
[39] A. M. Menzel, A. Saha, C. Hoell, and H. Löwen, J. Chem. Phys. **144**, 024115 (2016).
[40] R. W. Nash, R. Adhikari, J. Tailleur, and M. E. Cates, Phys. Rev. Lett. **104**, 258101 (2010).
[41] L. Durlofsky, J. F. Brady, and G. Bossis, J. Fluid Mech. **180**, 21 (1987).
[42] V. Gyrya, I. S. Aranson, L. V. Berlyand, and D. Karpeev, Bull. Math. Biol. **72**, 148 (2010).
[43] K. Drescher, R. E. Goldstein, N. Michel, M. Polin, and I. Tuval, Phys. Rev. Lett. **105**, 168101 (2010).
[44] J. S. Guasto, K. A. Johnson, and J. P. Gollub, Phys. Rev. Lett. **105**, 168102 (2010).
[45] J. Dunstan, G. Miño, E. Clement, and R. Soto, Phys. Fluids **24**, 011901 (2012).
[46] P. Mueller and J.-L. Thiffeault, Phys. Rev. Fluids **2**, 013103 (2017).
[47] J. de Graaf, H. Menke, A. J. Mathijssen, M. Fabritius, C. Holm, and T. N. Shendruk, J. Chem. Phys. **144**, 134106 (2016).
[48] D. Pimponi, M. Chinappi, P. Gualtieri, and C. M. Casciola, J. Fluid Mech. **789**, 514 (2016).
[49] E. M. Purcell, Am. J. Phys. **45**, 3 (1977).
[50] Angluar velocity of the swimmer generated by the flow $\mathbf{u}_0(\mathbf{r})$ is $(1/2)\nabla_{r_{\rm cm}} \times \mathbf{u}_0(\mathbf{r}_{\rm cm})$ [35]. This equates to zero, as can be seen by evaluating the curl, because the point force $\mathbf{f}^{\rm spc} = -f^{\rm sp}\hat{\mathbf{n}}$ points along a radial direction for the swimmer.
[51] Here we use the result of the integration of the Oseen tensor over a sphere $\oint_S dS\mathbf{T}(\mathbf{r}_S - \mathbf{r}'_S) = \mathbf{I}2a/3\eta$, where both $\mathbf{r}_S$ and $\mathbf{r}'_S$ are points on the surface of the sphere of radius a [35].
[52] Y. O. Fuentes, S. Kim, and D. J. Jeffrey, Phys. Fluids **31**, 2445 (1988).
[53] S. E. Spagnolie and E. Lauga, J. Fluid Mech. **700**, 105 (2012).
[54] J. Blake, J. Fluid Mech. **46**, 199 (1971).
[55] T. Bickel, A. Majee, and A. Würger, Phys. Rev. E **88**, 012301 (2013).
[56] T. C. Adhyapak and S. Jabbari-Farouji (unpublished).